

Figure 2: Differences in dose calculated on cCT and CBCT. Parameters calculated are D_{95} and mean dose for CTV-T and CTV-N, dose in the 1% receiving the highest dose for esophagus, bronchi and spinal cord, and dose in the volume receiving 20 Gy on the cCT for the lungs. Red lines denote the median, boxes the 25th to 75th percentiles and crosses outliers. Asterisks denote the structures that show a significant deviation from zero ($p < 0.05$, Wilcoxon signed rank test).

Conclusion

On an anthropomorphic phantom the error in dose calculated on CBCT is within 1%; this error is 2% larger going from phantom to patient images. Thus dose calculations on CBCT are feasible within ~3% accuracy when transferring structures rigidly between similar images.

Proffered Papers: PH 8: 4D imaging and motion management

OC-0411 Investigation of MRI-derived surrogate signals for modelling respiratory motion on an MRI-Linac

E.H. Tran¹, B. Eiben¹, A. Wetscherek², D.J. Collins², U.

Oelfke², G. Meedt³, D.J. Hawkes¹, J.R. McClelland¹

¹University College London, Medical Physics and Biomedical Engineering, London, United Kingdom

²The Institute of Cancer Research and The Royal Marsden NHS Foundation Trust, Joint Department of Physics, London, United Kingdom

³Elekta, Medical Intelligence Medizintechnik GmbH, Schwabmünchen, Germany

Purpose or Objective

Elekta's MRI-Linac combines a linear accelerator (linac) with a 1.5T MRI scanner enabling imaging of a patient's internal anatomy during radiotherapy treatment. Surrogate-driven motion models relate the motion of internal anatomy to easily measurable surrogate signal(s). Surrogates may therefore play a viable role in the realisation of online tracking and gating techniques in the MRI-Linac workflow. In this work, we generated and compared several MRI-derived respiratory surrogate signals to determine the most suitable one(s) for driving 2D motion models.

Material and Methods

Sagittal cine-MR images of two patients with advanced lung cancer were acquired at two alternating fixed slice locations through the tumour volume (Fig. 1a-b), with images from one location forming the surrogate dataset, and images from the other location forming the model dataset. The surrogate dataset was processed to generate signals based on the motion of diaphragm and skin, mean image intensity, image entropy, and principal component analysis (PCA) of the image intensities (Fig. 1c-d). Group-wise deformable image registration was performed on the model dataset to obtain deformation vector fields (DVF) which represent the motion measurements of the internal

anatomy. The model dataset was subdivided into training set and test set. The former was used to fit different multiple-signal linear correspondence models. Each model produced motion estimates by taking the surrogate signals as inputs and was evaluated calculating the deformation field error (DFE), which is the difference between the DVF estimated by the model and the DVF obtained from the group-wise registration.

Results

Table 1 gives the mean, standard deviation (std), and 95th percentile of the L2 norm of the DFE over all pixels within the body, averaged over all test images, as well as the maximum DFE over all pixels and images. The most accurate motion model for both patients is driven by three surrogate signals given by the scores of the first three principal components (PC), with average-mean DFE values of 0.5-0.6 mm. The maps of the loadings of the first PC (Fig. 1e-f) show that for both patients the diaphragm, lung vessels, and skin surface make a large contribution to the signal. However, for patient 2 the heart also makes a large contribution to the signal, and as a result the surrogate signal includes cardiac as well as respiratory components.

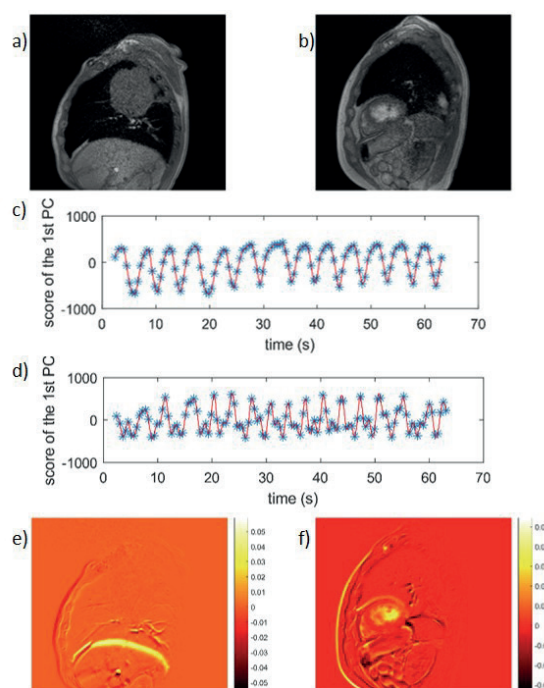


Figure 1. a)-b) Examples of sagittal MR images of the surrogate dataset for patient 1 and 2 respectively, acquired with a 1.5 T Siemens MRI scanner using a GRE sequence. Slice thickness: 10 mm, in-plane resolution: 1.98 mm x 1.98 mm. c)-d) Surrogate signals given by the scores of the first PC obtained applying PCA to the image intensities for patient 1 and patient 2 respectively. e)-f) Maps of the loadings of the first PC for patient 1 and patient 2 respectively.

Surrogate Signals	Patient 1				Patient 2			
	Mean (mm)	Std (mm)	Max (mm)	95 th tile (mm)	Mean (mm)	Std (mm)	Max (mm)	95 th tile (mm)
Diaphragm signal + its temporal derivative	0.64	0.44	4.57	1.47	0.67	0.67	6.61	2.09
Skin signal + its temporal derivative	0.97	0.89	7.07	2.85	0.68	0.69	6.35	2.17
Mean image intensity + its temporal derivative	0.94	0.77	6.61	2.54	0.91	0.82	8.82	2.65
Image entropy + its temporal derivative	1.07	0.93	9.90	3.04	0.8	0.77	7.26	2.45
Scores of the 1 st PC + its temporal derivative	0.65	0.45	4.06	1.50	0.75	0.74	7.01	2.36
Diaphragm signal + skin signal	0.56	0.44	4.87	1.43	0.66	0.65	5.93	2.06
Scores of the 1 st PC + scores of the 2 nd PC	0.63	0.46	5.75	1.51	0.61	0.61	7.30	1.91
Scores of the 1 st PC + scores of the 3 rd PC	0.53	0.38	4.09	1.25	0.76	0.76	6.76	2.41
Scores of the 1 st PC + scores of the 2 nd PC + scores of the 3 rd PC	0.49	0.35	3.85	1.17	0.59	0.59	7.06	1.85

Table 1. Summary statistics for the L2 norm of the DFE for all surrogate signals investigated to drive motion models for both patients. The mean, standard deviation and 95th percentile DFE values over all pixels were averaged over all test images, while the maximum DFE value over all test images was considered for the maximum values over all pixels. The scores of the 1st, 2nd and 3rd PC were obtained applying PCA to the image intensities.

Conclusion

PCA applied to the image intensities provides MRI-derived surrogate signals that give good results when modelling the 2D motion of the internal anatomy from a single slice. Future work will investigate other methods to generate surrogate signals, such as PCA applied to the DVFs, and will use additional 2D datasets from more lung cancer patients. Furthermore, the surrogate-driven motion models will be extended to include the 3D motion of the full anatomy enabling retrospective off-line estimation of the actual delivered dose.

OC-0412 Mechanically-assisted and non-invasive ventilation: Innovative step forward in the motion management

G. Van Ooteghem^{1,2}, D. Dasnoy-Sumel³, G. Lemaire⁴, G. Liistro⁵, E. Sterpin¹, X. Geets^{1,2}

¹Université Catholique de Louvain UCL - Institut de Recherche Expérimentale et Clinique IREC, SSS/IREC/MIRO Molecular Imaging- Radiotherapy and Oncology, Brussels, Belgium

²Cliniques Universitaires Saint Luc, Radiation Oncology, Brussels, Belgium

³Université Catholique de Louvain UCL, ImagX-R, Louvain-La-Neuve, Belgium

⁴Cliniques Universitaires Saint Luc, Anesthesiology, Brussels, Belgium

⁵Cliniques Universitaires Saint Luc, Pneumology, Brussels, Belgium

Purpose or Objective

Management of breathing-related motion remains challenging. Current strategies rely either on dedicated margins (ITV, MidPosition) that result in futile irradiation of normal tissues, or on respiratory-synchronized techniques that are highly sensitive to changes in breathing pattern and technologically exacting. Therefore, mechanically-assisted and non-invasive ventilation (MANIV) could be used on unsedated patients to impose regular breathing and reproducible tumour motion, but also to modulate the breathing pattern for motion mitigation techniques. We investigated the feasibility of MANIV on volunteers, and its impact on internal motion.

Material and Methods

Twelve healthy volunteers underwent 2 sessions of dynamic MRI, repeated over a few days. Each session was divided in 4 acquisitions of 15 minutes with 4 ventilation modes: spontaneous mode (SP), volume-controlled mode (VC) that imposes regular breathing in physiologic conditions, shallow-controlled mode (SH) that intends to lower motion amplitudes when increasing the breathing

rate up to 30 breaths per minute, and slow-controlled mode (SL) that mimics repeated end-inspiratory breath-holds (Figure 1). The last 3 modes were achieved under respirator without sedation. The motion of the diaphragm was tracked and expressed in position, amplitude, period and plateau during each MRI (intra-session analysis) and between MRI (inter-session analysis).

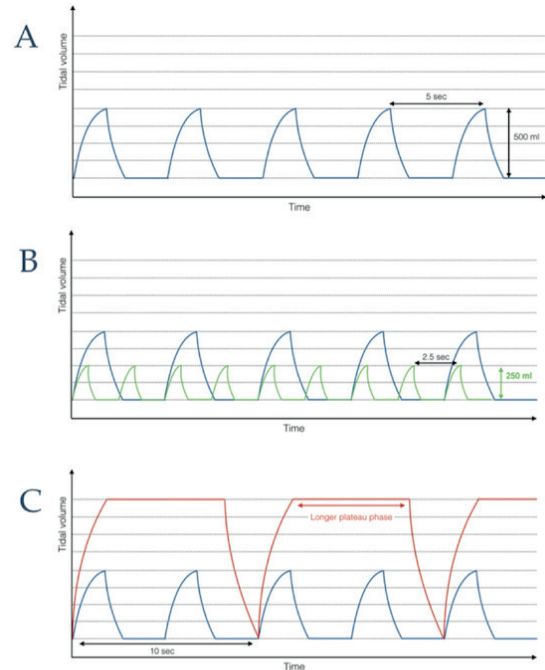


Figure 1 : (A) VC imposes a regular breathing rate and inhale volumes. (B) Increased breathing rate in SH allows smaller inhale volumes. (C) The end-inspiratory plateau in SL mimics repeated breath-holds.

Results

Intra-session analysis: Breathing rate variation was reduced in 97.92 % of cases with VC and SH compared to SP, with a mean reduction of 61.84 % \pm 22.23. The mean amplitude variation was decreased in 62.5 % of cases. Furthermore, amplitudes were systematically reduced with SH compared to VC, with a mean reduction of 12.22 mm \pm 6.4 (range: 5.2 - 27 mm) (Figure 2). In the SL mode, the mean variation of the plateau position was 4.84 mm \pm 3.53 (range: 2.27 to 12.72 mm) with 66.66 % of the volunteers achieving a variation smaller than 5 mm.

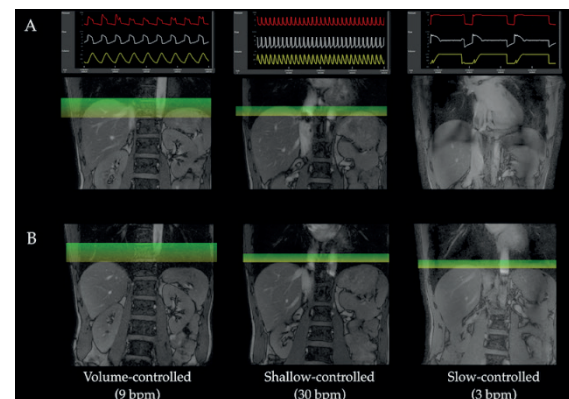


Figure 2 : (A) End-expiratory phases in VC, SH, SL modes. (B) End-expiratory phases in VC, SH, SL modes. The green windows highlight the smaller amplitude obtained with the SH mode compared to the VC mode and the residual motion during the end-inspiratory plateau with the SL mode.

Inter-session analysis: Compared to SP, VC and SH reduced both the mean breathing rate variation (0.72 vs 0.01 and 0.02 sec, respectively) and the mean amplitude variation (3.6 vs 2.51 and 1.78 mm, respectively) between the two MRI sessions. For SL, the mean variation of the plateau positions was 6.08 mm \pm 6.03 (range: 0.08